CHEMISTRY OF MATERIALS

pubs.acs.org/cm

Article

Microscopic Insights into the Reconstructive Phase Transition of $KNaNbOF_5$ with ^{19}F NMR Spectroscopy

Po-Hsiu Chien,[▽] Jaye K. Harada,[▽] Haoyu Liu,[▽] Sawankumar Patel, Chen Huang, James M. Rondinelli,* Kenneth R. Poeppelmeier,* and Yan-Yan Hu*

Cite This: *Chem. Mater.* 2020, 32, 5715−5722

Read Online

ACCESS | Metrics & More | Article Recommendations | Supporting Information

ABSTRACT: The centrosymmetric polymorph of $KNaNbOF_5$ undergoes a reconstructive transition from a rare A-site vacancy ordered perovskite to a unique nonperovskite high-temperature phase. Previously, the high temperature phase was proposed to exhibit dynamical disorder with mixed occupancy of O and F on the anion sites owing to hopping rotations of the $[NbOF_5]^{2-}$ octahedra. Here, we utilize ^{19}F NMR techniques to assess the dynamic anion configurations through this reconstructive transition. We conclude from these measurements that the high-temperature phase exhibits *Cmcm* symmetry with hopping rotations of the $[NbOF_5]^{2-}$ octahedra occurring only about the F_{apical}−Nb−O axis of the octahedra such that there are no O/F mixed occupancy anion sites. We use these results to refine the microscopic description of the reconstructive transition and its driving force and examine changes in the electronic structure of the d^0 oxyfluoride through the transition. Our work demonstrates the efficacy of ^{19}F NMR techniques combined with electronic structure calculations to understand thermodynamically driven changes in heteroanionic materials.

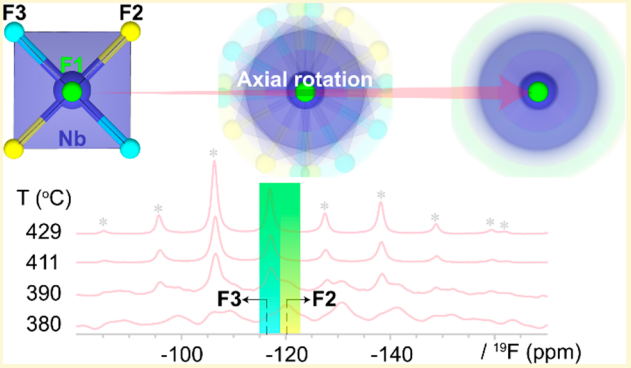

Downloaded via FLORIDA STATE UNIV on September 1, 2020 at 12:59:34 (UTC).
See https://pubs.acs.org/sharingguidelines for options on how to legitimately share published articles.

INTRODUCTION

Heteroanionic materials (HAMs) are an emerging class of designer materials in which functional properties can be tailored through insertion or exchange of a secondary anion.[1,2] Among the breadth of properties that are accessible through anion engineering are nonlinear optical properties such as second harmonic generation,[3] colossal magnetoresistance,[4] metal−insulator transitions,[5] and quantum phases.[6] A major obstacle to achieving these anion-enabled properties lies in understanding how to control and characterize anion ordering in HAMs, as long-range anion order is a key factor in the appearance (or lack thereof) of many acentric functional properties.[7] For example, anion ordering lifts inversion symmetry in $Na_3MoO_3F_3$, which is a necessary geometric requirement for ferroelectricity, piezoelectricity, and second harmonic generation. Anion disorder, likewise, can lead to unexpected responses as in Sr_2NiO_3F, whose low temperature spin-glass state arises in part due to the lack of anion ordering on the apical sites of the $[NiO_5F]^{7-}$ octahedra.[8] Additionally, different anion configurations can effect electronic and optical properties such as the band gap, which in computational studies of $CaTaO_2N$, was found to vary up to 0.6 eV depending on the anion configuration.[9] To that end, proper characterization of anion order is necessary to inform experimental synthesis and understand the origin of the macroscopic properties. Commonly utilized structural characterization techniques such as X-ray and neutron diffraction, however, may not be sufficient to determine the anion order of heteroanionic materials, especially in oxyfluorides where the scattering lengths of O and F are comparable.[1,2] Additional characterization techniques, such as IR, Raman, NMR spectroscopy, and electron diffraction are needed to accurately assess the extent of long-range and short-range order of multiple anions.

Specifically, ^{19}F NMR and powder X-ray diffraction (PXRD) have been used to synergistically determine the anion order in multiple oxyfluorides.[10−16] Advanced NMR techniques can also reveal more detailed anion ordering information. For example, in $Na_5W_3O_9F_5$, ^{19}F and ^{23}Na MAS, $^{23}Na \rightarrow {}^{19}F$ CP, and $^{19}F \rightarrow {}^{23}Na$ HETCOR NMR experiments were performed to further refine the anion site order determined by powder XRD and Raman spectroscopy studies and provided additional insight into the ferroelectric-ferroelastic properties of the material.[13] Additionally, NMR techniques have been used to study dynamic phenomena in oxyfluorides, such as dynamically

Received: April 3, 2020
Revised: May 20, 2020
Published: May 21, 2020

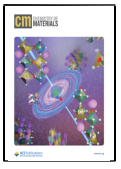

ACS Publications

© 2020 American Chemical Society

https://dx.doi.org/10.1021/acs.chemmater.0c01439
Chem. Mater. 2020, 32, 5715−5722

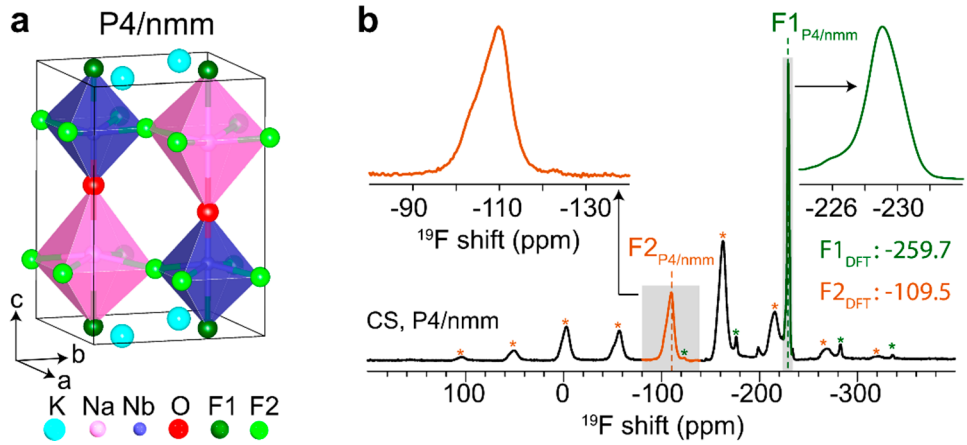

Figure 1. (a) Crystal structure and (b) high-resolution ^{19}F MAS (25 kHz) NMR spectrum of centrosymmetric (CS) $KNaNbOF_5$ (*P*4/*nmm*). In panel b, calculated ^{19}F NMR chemical shifts are also shown for reference. Asterisk (*) denotes spinning side bands.

disordered phases and order/disorder phase transitions.[17,18] For example, it was previously thought that the centrosymmetric to non- centrosymmetric phase transition in $K_3WO_3F_3$ from a disordered cryolite structure, $Fm\bar{3}m$, to the low temperature *I*4*mm* phase was due to ordering of the anion sites. Using a combination of variable-temperature Raman and ^{19}F NMR spectroscopy, it was found that the anion sites remain disordered across the transition owing to fast reorientations of the fac-$[WO_3F_3]^{3-}$ octahedra.[17]

Here we use NMR techniques to examine the microscopic origins of an unusual reconstructive phase transition[19] in the oxyfluoride $KNaNbOF_5$. The room-temperature centrosymmetric variant of $KNaNbOF_5$ is an anion ordered elpasolite with ordered A-site vacancies. Upon heating from this tetragonal *P*4/*nmm* structure, reconfiguration of the cation sublattice (and its associated vacant sites) occurs with rotations of nearly rigid $[NbOF_5]^{2-}$ octahedra breaking K/Na-ligand bonds. This complex choreography was proposed to rely on hopping rotations between six stable orientations of the $[NbOF_5]^{2-}$ octahedra, which effectively alter the O and F site order as seen from synchrotron powder X-ray diffraction (PXRD) measurements, and was proposed to yield a dynamically disordered high temperature (HT) phase with orthorhombic *Cmcm* symmetry. Specifically, the dynamic disorder refers here to a state with an average structure consisting of a mixture of two phases distinguishable at the unit cell level with *Pbcm* and *Pnma* symmetry identified from molecular dynamics simulations. The *Cmcm* structure forms a supergroup connecting these two phases. Using high-resolution and high-temperature ^{19}F magic-angle-spinning (MAS) NMR and density functional theory calculations, we show that HT phase is unlikely dynamically disordered between two phases and can be described with *Cmcm* symmetry. We show that the rotational hopping of the $[NbOF_5]^{2-}$ octahedra is limited to rotations about the F_{apical}–Nb–O axis of the octahedra, indicating that the HT phase does not show mixed anion-site occupancy, all anion sites are either 100% O or 100% F. Additionally, we connect the structural changes of the heteroleptic oxyfluoride units through the reconstructive transition to changes in the calculated electronic band gap. Last, we revise the model and driving force for the reconstructive transition in $KNaNbOF_5$, arguing that it originates from only hopping rotations (orientational disorder) rather than O/F disorder on the anion sites.

RESULTS AND DISCUSSION

The crystal structure and high-resolution ^{19}F MAS NMR spectrum of centrosymmetric (CS) $KNaNbOF_5$ (*P*4/*nmm*) are shown in Figure 1. In CS KNaNbOF5 (Figure 1a), two distinct F atoms are identified in the $[NbOF_5]^{2-}$ octahedra: the apical and equatorial fluorine atoms. The apical fluorine atom ($F1_{P4/nmm}$; notation of $F(\#)_{space\ group}$ is used to indicate specific fluorine anion sites in different phases of $KNaNbOF_5$ throughout) sits parallel with O along the *c*-direction or trans to O, whereas the equatorial fluorine atom ($F2_{P4/nmm}$) connects the $[NaOF_5]^{6-}$ and $[NbOF_5]^{2-}$ octahedra in the *ab*-plane.[19] The ratio of site multiplicities between $F1_{P4/nmm}$ and $F2_{P4/nmm}$ is 1:4 with 100% site occupancy indicating anion order and resulting in the stoichiometry of 5 for the fluorine atom in the CS polymorph of $KNaNbOF_5$.

The high-resolution ^{19}F MAS (25 kHz) NMR spectrum of the CS form of $KNaNbOF_5$ is shown in Figure 1b. Two ^{19}F isotropic NMR resonances, determined by recording ^{19}F NMR spectra at different MAS rates where isotropic resonances do not vary their positions with spinning (Figure S1), appear at −229.2 and −109.5 ppm, respectively. The ratio of the ^{19}F NMR spectral areal integral (including associated spinning side bands) of the resonances at −109.4 and −229.2 ppm is 1:4, which agrees well with the multiplicities of two fluorine atoms in the CS form of $KNaNbOF_5$. Thus, the ^{19}F resonance at −229.2 ppm is assigned to the crystallographically distinct apical $F1_{P4/nmm}$ atom, and the ^{19}F resonance at −109.5 ppm is assigned to the equatorial $F2_{P4/nmm}$ atom. This assignment is also supported by DFT ^{19}F NMR calculations (Table S1).

The equatorial fluorine atom ($F2_{P4/nmm}$) showing a ^{19}F NMR resonance at −109.5 ppm presents a pronounced asymmetric line shape with an estimated full width at half-maximum (fwhm) of 4.3 kHz. Since the X-ray diffraction data[20] only reveals one type of local environment (Wyckoff site: 8*j*) for the equatorial fluorine atom, this wide distribution of ^{19}F frequencies is attributed to NMR interactions. In fact, ^{93}Nb–^{19}F J-coupling and residual ^{93}Nb–^{19}F dipolar coupling have been claimed and verified as the origin for this asymmetry in the ^{19}F signal of $Cdpy_4NbOF_5$.[16] In $KNaNbOF_5$, the shorter Nb–$F2_{P4/nmm}$ bond (1.95 Å) makes the through-bond ^{93}Nb–^{19}F J-coupling more noticeable than that of the Nb–$F1_{P4/nmm}$ bond (2.15 Å), although the multiplet pattern is not resolved in either resonance likely due to residual broadening resulting from dipolar coupling interactions and relaxation.

https://dx.doi.org/10.1021/acs.chemmater.0c01439
Chem. Mater. 2020, 32, 5715−5722

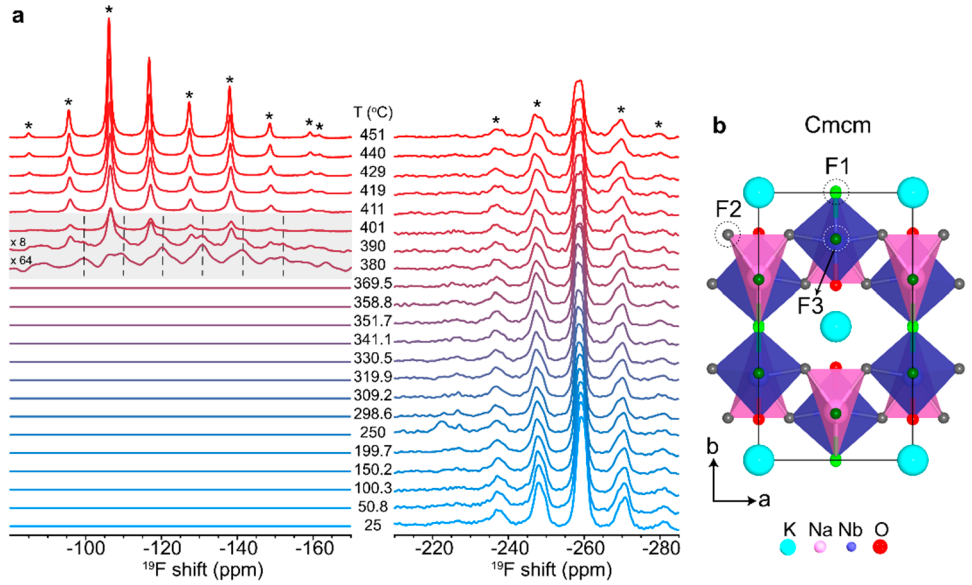

Figure 2. (a) In situ monitoring (heating process) of the phase transition in $KNaNbOF_5$ from the centrosymmetric (CS) phase (*P4/nmm*) to the high-temperature (HT) phase (*Cmcm*) by variable-temperature ^{19}F MAS (5 kHz) NMR. (b) Crystal structure of *Cmcm* $KNaNbOF_5$. Asterisk (*) denotes spinning side bands. Dashed lines serve as a guide-to-the-eye.

Note, the line broadening we observe is not relevant to understanding the reconstructive phase transition of $KNaNbOF_5$ and thus we do not assess it further.

To follow the structural changes in the $[NbOF_5]^{2-}$ unit during the CS → HT phase transition, in situ high-temperature ^{19}F MAS (5 kHz) NMR is employed, and the summarized ^{19}F spectra following the heating process are presented in Figure 2 (the cooling process is shown in Figure S2). It is worth pointing out that this temperature-dependent ^{19}F NMR study was performed at a MAS rate of 5 kHz, due to hardware limitations for high-temperature NMR. Therefore, the spectra in Figure 2 show poorer resolution compared with spectra acquired at 25 kHz as shown in Figure 1. In the ^{19}F spectrum acquired at room temperature, one resonance appears at −259.2 ppm with a slightly asymmetric line shape, which agrees with the calculated shift of the apical fluorine ($F1_{P4/nmm}$) atom in CS $KNaNbOF_5$ (−259.7 ppm; Table S1). As a result, this −259.2-ppm resonance is assigned to $F1_{P4/nmm}$. The asymmetric line shape for the −259.2-ppm peak may arise from the J-coupling between Nb and the apical $F1_{P4/nmm}$. The large chemical shift anisotropy (CSA) of the ^{19}F resonance of equatorial fluorine atoms, $F2_{P4/nmm}$, renders the signal invisible at low spinning rates. To prove this, the magnitude of CSA is obtained by quantitatively simulating the high-resolution ^{19}F NMR spectrum of $KNaNbOF_5$ acquired at a fast MAS rate of 25 kHz (Figure 1b), and the CSA values of $F2_{P4/nmm}$ and $F1_{P4/nmm}$ ^{19}F resonances are 183.5 kHz and 21.9 kHz, respectively. The large shift anisotropy spreads out the ^{19}F signal of $F2_{P4/nmm}$ over a very broad range >180 kHz at low spinning rates, e.g., 5 kHz, resulting in extremely low sensitivity.

Upon increasing temperature to 369.5 °C, no noticeable changes in the chemical shift or line width can be seen in the ^{19}F spectra, except for minor short-range structural adjustments occurring at 250 °C, manifested in the appearance of small resonances at −223 ppm. Similar changes are observed for minor resonances near −211 ppm during the cooling process at a lower temperature of 199.7 °C (Figure S2). Whether these structural adjustments are necessary before the phase transition takes place are not clear at this stage. Note that these structural changes should not interfere with the following discussion as we will show that at temperatures below 370 °C, no discernible phase transition can be traced. The unaltered line width of the $F1_{P4/nmm}$ resonance from room temperature to 369.5 °C implies negligible F-ion motion, suggesting improbable O/F site disorder in the $[NbOF_5]^{2-}$ unit within the low-temperature range.

At 380 °C, two ^{19}F resonances emerge at −120.2 and −116.7 ppm. According to DFT ^{19}F NMR calculations of different $KNaNbOF_5$ phases (Table S1), these two resonances originate from equatorial fluorine atoms ($F2_{Cmcm}$ and $F3_{Cmcm}$) in the high-temperature phase (*Cmcm*). The emergence of these two ^{19}F resonances signifies the transition of $KNaNbOF_5$ from the centrosymmetric phase (*P4/nmm*) to the high-temperature phase (*Cmcm*). In these two phases, the local coordination of the apical fluorine atom, excluding site symmetry, is unchanged. The $F1_{P4/nmm}$ and $F1_{Cmcm}$ can be viewed as the bridging atom between the Nb and Na polyhedra, and both atoms are trans to O as in the $[NbOF_5]^{2-}$ octahedra (Figures 1a and 2b). This similarity in the connectivity of the apical fluorine atom with Nb and Na in each corresponding polymorph results in the same ^{19}F chemical shift at −259.7 ppm. In contrast, the local environment of the equatorial fluorine atoms is substantially different because of the change in molecular ge-ometry of the Na polyhedra from a distorted octahedron, $[NaOF_5]^{6-}$, to distorted trigonal bipyramid, $[NaF_5]^{4-}$, in the CS → HT phase transition. The difference in local coordination of the equatorial fluorides in the HT phase leads to the formation of two distinct groups of equatorial fluorine atoms ($F2_{Cmcm}$ and $F3_{Cmcm}$) as revealed by a small difference in ^{19}F NMR resonances (Figure 2).

As the temperature ramps up higher than 380 °C, the ^{19}F signals of the two equatorial fluorine atoms gradually merge, likely owing to fast F-ion exchange between them, rendering a sharp resonance at −116.7 ppm when the temperature reaches 450 °C. The averaged single ^{19}F isotropic shift of equatorial

https://dx.doi.org/10.1021/acs.chemmater.0c01439
Chem. Mater. 2020, 32, 5715−5722

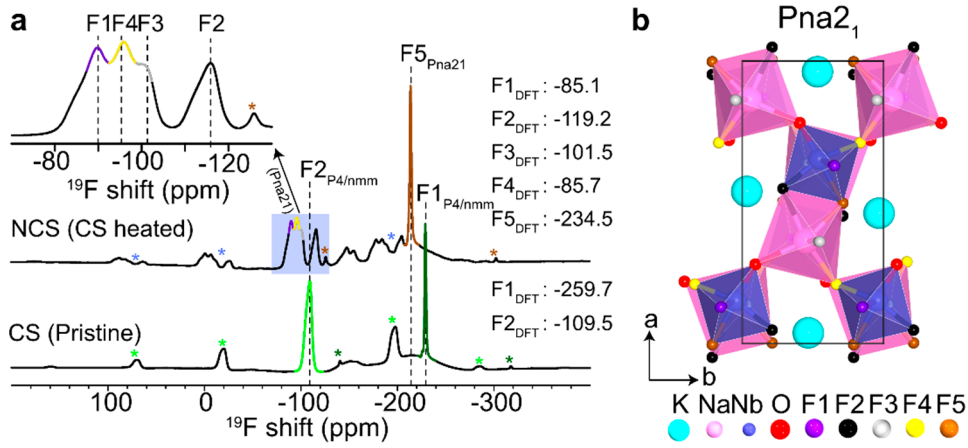

Figure 3. (a) High-resolution ^{19}F MAS (50 kHz) NMR spectra before and after heat-treatment on CS $KNaNbOF_5$. (b) Crystal structure of noncentrosymmetric (NCS) $KNaNbOF_5$ ($Pna2_1$). In panel a, calculated ^{19}F NMR chemical shifts are also shown for reference. Asterisk (*) denotes spinning side bands.

fluorine atoms (F_{Cmcm}) at 450 °C is further verified as shown in Figures S3 and S4.

These findings indicate that the HT structure is not a dynamically disordered state between the previously proposed *Pnma* and *Pbcm* phases. The structures of the *Pnma* and *Pbcm* phases are shown in Figure S5 and both have an additional crystallographic fluorine site. DFT ^{19}F NMR calculations on *Pnma* and *Pbcm* phases suggest that isotropic ^{19}F NMR shifts (Table S1) of the equatorial fluorine sites resonate at −124.2, −94.7, and −93.6 ppm for *Pnma* and −140.6, −108.4, and −84.8 ppm for *Pbcm* (Table S1). However, these resonances are not experimentally observed. At 380 °C and above, we do not observe more than three peaks in the spectra or peaks greater than −110 ppm, indicating that the high temperature phase is likely only *Cmcm*.

Considering the fact that both the resonance position and line width of the apical fluorine atom ($F1_{Cmcm}$) are temperature independent, the motion-induced narrowing following the coalescence of the ^{19}F peaks (equatorial $F2_{Cmcm}$ and $F3_{Cmcm}$) suggests that the hopping rotations of the $[NbOF_5]^{2-}$ unit are restricted to rotations about the F_{apical}−Nb−O axis (vide infra). This means that only the equatorial F atoms are allowed to swap positions and no O/F site disorder is possible.[21] To further validate this statement, DFT ^{19}F NMR shift calculations on the HT phase (*Cmcm*) of $KNaNbOF_5$ is performed using an axial model, where the positions of the equatorial fluorine atoms are swapped, and a free rotation model, where the positions of one apical oxygen and one equatorial fluorine atom were swapped to mimic O/F site disorder. The result of this computational work is presented in Table S2. Examining individual F sites, the ones that change the most are F9 corresponding to the position of the apical oxygen, F1, which now is located trans to a F rather than O in the $[NbOF_5]^{2-}$ octahedra, and F11, which rests in an equatorial F position, but is now trans to an O in $[NbOF_5]^{2-}$. The apical F sites, F1 and F9, show downfield shifting to −133.1 ppm and −80.1 ppm, respectively, while the equatorial F11 shows upfield shifting to −166.4 ppm. Averaging over apical and equatorial sites, this manifests as a significant downfield shifting (larger ppm) in the averaged ^{19}F chemical shift of the apical fluorine atom (−204.5 ppm) in the free rotation model. In the case of axial rotations about the F_{apical}−Nb−O axis, the exchange of equatorial fluorine atoms does not shift the ^{19}F resonances, and the apical fluorine atom resonates with an average value at −221.2 ppm, which is more comparable to the experimental shift at −257.4 ppm (Table S1). Therefore, O/F site disorder (i.e., free rotations) is unlikely to occur in the HT form of $KNaNbOF_5$ since our experimental ^{19}F chemical shifts contradict the predicted chemical shifts in the presence of free rotations (hopping of the $[NbOF_5]^{2-}$ octahedra about six symmetry equivalent configurations).

During the cooling process (Figure S2), the sharp ^{19}F resonance (−116.7 ppm) at high temperature abruptly splits into two peaks as the temperature decreases to 380−370 °C, which is in line with the reduced F motion associated with the axial rotation of the $[NbOF_5]^{2-}$ unit. Below 370 °C, ^{19}F signals representing the equatorial fluorine atoms fade away due to an insufficient MAS rate for averaging the regained large CSA. High-resolution MAS NMR at 50 kHz is employed to determine the room-temperature phase after cooling.

High-resolution ^{19}F MAS NMR spectra acquired at a spinning rate of 50 kHz of the heat-treated $KNaNbOF_5$ after cooling to room temperature and the pristine CS $KNaNbOF_5$ are shown in Figure 3. In contrast to the spectrum for the CS form of $KNaNbOF_5$, the ^{19}F MAS spectrum of the heated sample reveals five individual ^{19}F peaks (Figure 3a, top panel), indicating that CS → HT transition is irreversible and a different phase of $KNaNbOF_5$ is obtained upon cooling, as previously observed in PXRD experiments.[19,23]

The experimental ^{19}F chemical shifts (Table S1) agree moderately well with the computed shifts in the non-centrosymmetric (NCS) form of $KNaNbOF_5$ ($Pna2_1$).[19,23] For the NCS form of $KNaNbOF_5$ (Figure 3b), five crystallographically distinct F sites are identified in the $[NbOF_5]^{2-}$ octahedra.[22] The ratio of the multiplicities among $F1_{Pna21}$, $F2_{Pna21}$, $F3_{Pna21}$, $F4_{Pna21}$, and $F5_{Pna21}$ is 1:1:1:1:1, and the site occupancy is 100% (i.e., anion ordered) for all of five sites. The percentage of the ^{19}F NMR resonance areal integral (including spinning side bands) of the apical F ($F5_{Pna21}$) over the sum of the other four equatorial fluorine atoms ($F1_{Pna21}$ to $F4_{Pna21}$) is 19.4% (∼ 1/5) and the integral ratio among $F2_{Pna21}$, $F3_{Pna21}$, $F4_{Pna21}$, and $F1_{Pna21}$ (from small to large ppm) is 1.02:0.83:1.13:1.15, roughly consistent with the expected ratio of multiplicities in the NCS form of $KNaNbOF_5$ ($Pna2_1$). We therefore assign the structure of the heat-treated

https://dx.doi.org/10.1021/acs.chemmater.0c01439
Chem. Mater. 2020, 32, 5715−5722

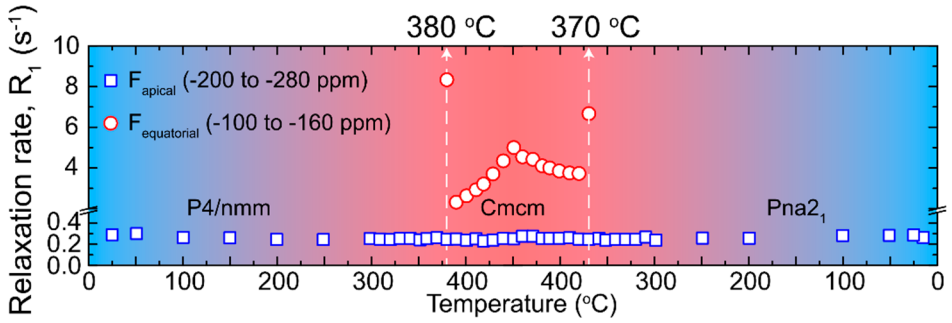

Figure 4. In situ ^{19}F NMR spin−lattice relaxation rate ($R_1 = 1/T_1$) measurements on the CS-to-HT phase transition upon heating (0 to 450 °C) and the HT-to-NCS transition upon cooling (450 to 0 °C) in $KNaNbOF_5$.

sample to the NCS phase and confirm that cooling $KNaNbOF_5$ from high temperature leads to a polymorphic transition to the ground state noncentrosymmetric nonperovskite polymorph.[19] We note that the $F5_{Pna21}$ site (Figure 3b), which is axially opposite to O in the $[NbOF_5]^{2-}$ unit, presents the most upfield chemical shift (smaller ppm), and the rest of four equatorial fluorine atoms ($F1_{Pna21}$ to $F4_{Pna21}$) share a wide distribution of chemical shifts in a range between −90 to −120 ppm. This is similar to what is observed in the CS structure, in which the apical fluorine atom ($F1_{P4/nmm}$) resonates at the most upfield and the equatorial one ($F2_{P4/nmm}$) downfield at −109.5 ppm.

We now examine the possibility of dynamic O/F site disorder in the $[NbOF_5]^{2-}$ unit. Ion dynamics often induces fluctuation in local magnetic field, resulting in loss of spin coherence and thus changes in spin relaxation times. Therefore, NMR relaxometry is a sensitive tool for probing ion dynamics. *In situ* high-temperature ^{19}F spin−lattice relaxation time (T_1) measurements are performed on CS (*P*4/*nmm*) $KNaNbOF_5$ and the results are given in Figure 4. The T_1 times of the equatorial fluorine atoms ($F2_{P4/nmm}$, $F2_{Cmcm}$, $F3_{Cmcm}$; red circles in Figure 4) cannot be determined until 380 °C as their ^{19}F signals are unobservable due to large CSA. The T_1 values of the apical (−200 ppm to −280 ppm) and the equatorial (−100 to −160 ppm) F show significant difference. In particular, the relatively long T_1 times (slower relaxation rate $1/T_1$, blue squares) of the apical fluorine atoms ($F1_{P4/nmm}$ and $F1_{Cmcm}$) in both phases are independent of temperature throughout the entire measurement. The lack of changes in long relaxation time and no narrowing of the CSA with temperature for the $F1_{P4/nmm}$ and $F1_{Cmcm}$ resonances suggest very little motion is associated with $F1_{P4/nmm}$ and $F1_{Cmcm}$. Combined with evidence of no shift changes in these resonances, no static or dynamic O/F disorder occurs in the high temperature phase.

The reconstructive phase transition is revealed by a sudden jump in the relaxation rate (R_1) from 380 to 390 °C. The abrupt change in T_1 upon heating indicates structural modification and suggests the completion of the $P4/_{nmm} \rightarrow$ *Cmcm* phase transition. The continuously shortened T_1 (increased relaxation rate $1/T_1$) from 390 to 450 °C, in conjunction with gradual reduction of CSA and narrowing of the isotropic resonance at −116.9 ppm (Figure S6), suggest increasing F exchange through axial rotations of the $[NbOF_5]^{2-}$ unit, which gradually averages out the CSA and the $^{19}F-^{19}F$ dipolar couplings (Figure S6). On the cooling process, a reversible behavior is seen with a slower rate and smaller change in amplitude (Figure 4) likely due to different transition pathways (*P*4/*nmm* → *Cmcm* vs *Cmcm* → $Pna2_1$) as the axial rotations of the $[NbOF_5]^{2-}$ unit in the CS (*P*4/*nmm*) and NCS ($Pna2_1$) form of $KNaNbOF_5$ cannot be identical. At 370 °C, the sharp change in T_1 times indicates another structural modification responsible for the *Cmcm* → $Pna2_1$ displacive phase transition. Based on the results of the in situ high-temperature ^{19}F T_1 measurements, the observed nature of dynamic disorder is confirmed as a result of rapid rotation in the $[NbOF_5]^{2-}$ unit about the axis of $F_{apical}-Nb-O$, and thus, no O/F anion disorder occurs in the high temperature phase.

Based on this understanding of the high-temperature structure and the associated thermally controlled structural dynamics, we propose a revised model for the reconstructive phase transition. Previously, the reconstructive transition was believed to be effectively driven by O/F site disorder induced by thermally driven octahedral hopping rotations among multiple symmetry equivalent orientations. Consequently, the anion disorder destabilizes the coordination environment of the K^+ and ordered vacant sites and leads to electrostatic interactions that cause them to attract.[19] Given our results, it is clear that O/F disordering is not active in *P*4/*nmm* → *Cmcm* transition. We propose the hopping rotations alone are enough to destabilize the coordination environment of the K^+ ions and thus, the ordered A-site vacancies. Given that this type of ordered vacancy has only been observed in a few heteroanionic materials and not at all seen in homoanionic materials (i.e., oxides),[20] we expect that this type of vacancy ordering is generally unfavorable or perhaps stabilized by the O/F anion ordering. We expect that other known perovskites with ordered A-site vacancies, such as $KNaMoO_2F_4$ and $KNaWO_2F_4$, may also show an irreversible reconstructive transition upon heating and a new phase upon cooling.

Last, our results are consistent with the minimum-energy-pathway (MEP) model for the reconstructive transition described previously (Figure S7a).[19] The structure proceeds from the *P*4/*nmm* phase to a structure very similar to the *Pbcm* phase and then to HT *Cmcm* structure. Given the confirmation of O/F order in this structure, we can ascertain the electronic structure dependencies due to these structural changes through the reconstructive transition with reasonable accuracy. Despite the reconstructive nature of the transition from the CS to HT phases in $KNaNbOF_5$, only minor changes in the calculated band gap are observed (4.32 and 4.30 eV, respectively). Interestingly, the band gap along the calculated MEP[18] changes more as the $[NbOF_5]^{2-}$ octahedra rotate through the transition (Figure S7b). Upon detailed inspection of the electronic structure in Figure S7c and the structures along the MEP, we find that the changes in the band gap are correlated

https://dx.doi.org/10.1021/acs.chemmater.0c01439
Chem. Mater. 2020, 32, 5715−5722

with the change in the bandwidth of the F p states, except between points C and D. As the structure initially distorts away from the CS phase (point A), its behavior is similar to a displacive transition in which rotations of octahedra increases the band gap slightly, as expected for perovskite-like heteroanionic materials.[24] Further along the transition pathway, between points B and C, the structure no longer appears perovskite-like as the Na−F bonds begin to break as the rigid $[NbOF_5]^{2-}$ octahedra rotate. The band gap slightly decreases again, due to a widening of the F p states due to a change in orbital overlap with Nb. An increase in band gap between C and D occurs because the rigid $[NbOF_5]^{2-}$ octahedra and distorted Na-polyhedra move toward sharing an edge, which decreases the ligand-field splitting of the Nb orbitals. Finally, as the structure distorts toward the *Cmcm* phase, the Nb- and Na-polyhedra become corner sharing, increasing the ligand-field splitting and increasing the band gap.

In addition to the $[NbOF_5]^{2-}$ octahedra maintaining their rigidity and largely rotating about the *c*-axis throughout the transition pathway, the K^+ cations displace along the *b*-axis, effectively merging with the A-site vacancies and eliminating them. This essentially eliminates the perovskite-like structure observed in *P*4/*nmm* and transitions to a new unique structure type. Interestingly, after the transition, the K^+ ion forms two bonds to O and this coordination persists upon cooling through the reversible transition to the thermodynamic NCS ground-state phase (Figure S8). These K−O bonds are not seen in the CS polymorph.

CONCLUSION

Using high-resolution and high-temperature ^{19}F MAS NMR, we have confirmed the irreversible, reconstructive phase transition in $KNaNbOF_5$ from the CS *P*4/*nmm* polymorph to the HT *Cmcm* phase. In addition, we clarify some previously unobserved dynamic phenomena in the high temperature phase. We showed the HT structure is likely one phase, *Cmcm*, rather than a dynamically disordered phase consisting of *Pbcm* and *Pnma*, as proposed previously. Additionally, we showed that in the HT structure, the hopping rotations of the $[NbOF_5]^{2-}$ octahedra only occur about the F_{apical}−Nb−O axis meaning that all of the anion sites are fully occupied by either F or O and hopping is only allowed between $F_{equatorial}$ sites. Based on these observations, we propose that the reconstructive transition in this perovskite with ordered A-site vacancies and ordered anions is driven by the axial rotations of the $[NbOF_5]^{2-}$ octahedra.

EXPERIMENTAL SECTION

Synthesis and Structure Confirmation of $KNaNbOF_5$. Caution: Hydrofluoric acid is toxic and corrosive and must be handled with extreme caution and the appropriate protective gear! If contact with the liquid or vapor occurs, proper treatment procedures should immediately be followed.[25−27]

The reagents NaF (99%, Aldrich), KNO_3 (99.9%, Mallinckrodt), Nb_2O_5 (99.5%, Strem), and aqueous hydrofluoric acid (HF; 48% HF by weight, Aldrich) were used as received. All reactants were sealed in Teflon pouches as previously described.[28] The precursor Na_2NbOF_5 was synthesized hydrothermally via a previously published procedure[23] by combining 0.1344 g of NaF, 0.4254 g of Nb_2O_5, and 1.2 mL of aqueous HF in a Teflon pouch. Six pouches were placed in a 125 mL Teflon-lined Parr pressure vessel filled with 42 mL of deionized water as backfill, and heated at 5 °C/min to 150 °C, held for 24 h, and slowly cooled to room temperature at 0.1 °C/min. The cooled products were left in the pouches at room temperature to crystallize over 2 weeks. The product was then recovered in air via vacuum filtration.

The CS phase was synthesized with 0.0550 g (2.20×10^{-4} mol) of Na_2NbOF_5, 0.0160 g (1.582×10^{-4} mol) of KNO_3, and 0.12 mL (6.7×10^{-3} mol) of H_2O. The reagents were sealed in Teflon pouches and heated using the same procedure as for the Na_2NbOF_5 precursor. Both the CS and NCS products were left to crystallize in the pouches for 1−2 weeks to increase yield before recovery by vacuum filtration. Sample purity was confirmed by powder X-ray diffraction measurements on an Ultima IV X-ray diffractometer (Rigaku) with Cu radiation. Powder patterns were analyzed using MDI Jade (2010).

Solid-State ^{19}F NMR Experiments. The local ^{19}F environments in $KNaNbOF_5$ are examined by solid-state ^{19}F magic-angle-spinning (MAS) NMR operating at 470.5 MHz (11.75 T) on a Bruker Avance-III 500 spectrometer, which is equipped with a 2.5 mm Bruker HXY probe. ^{19}F spectra are obtained using a rotor-synchronized spin−echo sequence with a 90° pulse of 2 μs and a recycle delay of 100 s at a spinning rate of 25 kHz. In case of signals overlapping between spinning side bands and isotropic shifts, ultrafast MAS ^{19}F measurements are performed using a Bruker 1.3 mm Bruker HXY probe operating at 564.6. MHz (14.1 T) on a Bruker Avance NEO 600 spectrometer at a spinning rate of 50 kHz. ^{19}F spectra are obtained using a single pulse of 2.8 μs and a recycle delay of 100 s.

The reconstructive phase transition (*P*4/*nmm* to *Cmcm*) is investigated with in situ (heating and cooling) high-temperature ^{19}F MAS NMR on the CS (*P*4/*nmm*) phase $KNaNbOF_5$. ^{19}F experiments are carried out using a LASMAS probe[29] operating at 470.5 MHz (11.75 T) on a Bruker Avance-III 500 spectrometer. ^{19}F spectra are collected from room temperature to 450 °C with rotor-synchronized spin−echo sequence using a 90° pulse of 6.9 μs and a recycle delay of 20 s at a spinning rate of 5 kHz. ^{19}F T1 relaxation measurements are performed with an inversion−recovery sequence to probe the behavior of F-ion dynamics. Prior to acquisitions of ^{19}F spectra, temperature calibration of the LASMAS probe is performed by linearizing the ^{79}Br chemical shift of KBr as a function of temperature (from room temperature to 700 °C).[30] After cooling, the heat-treated $KNaNbOF_5$ are subject to high-resolution ^{19}F MAS (25 or 50 kHz; 2.5 mm or 1.3 mm HXY probe) NMR to examine the ^{19}F local environments for phase identification. All ^{19}F spectra were calibrated with $LiF_{(s)}$ at −201 ppm. All ^{19}F spectra were analyzed and processed on Topspin (v4.0).

^{19}F NMR Shift Calculation. All of the calculations based on DFT were performed in the Vienna ab initio simulation package (VASP).[31] The crystal structures of the CS and NCS phases were retrieved from ref 32. The structures of the HT phases (*Cmcm*, *Pnma*, and *Pbcm*) were retrieved from ref 19. The structure information on intermediate phases was obtained from group theoretical method and density functional theory (DFT) methods described in previous work.[19] Projector-augmented-wave approach was used for electronic structure calculations with Perdew−Burke−Ernzerhof generalized-gradient approximation (PBE-GGA).[33,34] A planewave cutoff of 500−550 eV and a k-point density of at least 500 per number of atoms in the unit cell were set until the total energy converged in all calculations. Before NMR shift calculation, the unit cell parameters were also relaxed. The chemical shifts were determined by magnetic shieldings using perturbation theory (linear response).[35,36] The calculated shifts matched well with experimental shifts with a calibration factor of +15 ppm.

ASSOCIATED CONTENT

Supporting Information

The Supporting Information is available free of charge at https://pubs.acs.org/doi/10.1021/acs.chemmater.0c01439.

Analysis of ^{19}F NMR spectra and DFT calculation on ^{19}F NMR shifts for $KNaNbOF_5$, electronic structure calculations of structures along the reconstructive transition path, and K^+ coordination (PDF)

https://dx.doi.org/10.1021/acs.chemmater.0c01439
Chem. Mater. 2020, 32, 5715−5722

AUTHOR INFORMATION

Corresponding Authors

James M. Rondinelli − *Department of Materials Science and Engineering, Northwestern University, Evanston, Illinois 60208, United States;* orcid.org/0000-0003-0508-2175; Email: jrondinelli@northwestern.edu

Kenneth R. Poeppelmeier − *Department of Materials Science and Engineering and Department of Chemistry, Northwestern University, Evanston, Illinois 60208, United States;* orcid.org/0000-0003-1655-9127; Email: krp@northwestern.edu

Yan-Yan Hu − *Department of Chemistry and Biochemistry, Florida State University, Tallahassee, Florida 32306, United States; Center of Interdisciplinary Magnetic Resonance, National High Magnetic Field Laboratory, Tallahassee, Florida 32310, United States;* orcid.org/0000-0003-0677-5897; Email: yhu@fsu.edu

Authors

Po-Hsiu Chien − *Department of Chemistry and Biochemistry, Florida State University, Tallahassee, Florida 32306, United States; Center of Interdisciplinary Magnetic Resonance, National High Magnetic Field Laboratory, Tallahassee, Florida 32310, United States;* orcid.org/0000-0002-1607-1271

Jaye K. Harada − *Department of Materials Science and Engineering, Northwestern University, Evanston, Illinois 60208, United States*

Haoyu Liu − *Department of Chemistry and Biochemistry, Florida State University, Tallahassee, Florida 32306, United States*

Sawankumar Patel − *Department of Chemistry and Biochemistry, Florida State University, Tallahassee, Florida 32306, United States*

Chen Huang − *Department of Scientific Computing, Florida State University, Tallahassee, Florida 32306, United States;* orcid.org/0000-0003-2934-8118

Complete contact information is available at: https://pubs.acs.org/10.1021/acs.chemmater.0c01439

Author Contributions

$^{\nabla}$P.-H.C., J.K.H., and H.L. contributed equally to this work.

Notes

The authors declare no competing financial interest.

ACKNOWLEDGMENTS

P.-H.C., J.K.H., J.M.R., K.R.P., and Y.-Y.H. were supported by NSF's MRSEC program (DMR-1720139) at the Materials Research Center of Northwestern University. H.L. acknowledges the support from the National Science Foundation (NSF) under the Grant No. 1847038. All solid-sate NMR experiments were performed at the National High Magnetic Field Laboratory, which is supported by National Science Foundation Cooperative Agreement No. DMR-1644779 and the State of Florida. This work made use of the Jerome B. Cohen X-ray Diffraction Facility supported by the MRSEC program of the National Science Foundation (DMR-1720139) at the Materials Research Center of Northwestern University and the Soft and Hybrid Nanotechnology Experimental (SHyNE) Resource (NSF ECCS-1542205.)

REFERENCES

(1) Harada, J. K.; Charles, N.; Poeppelmeier, K. R.; Rondinelli, J. M. Heteroanionic Materials by Design: Progress Toward Targeted Properties. *Adv. Mater.* **2019**, *31* (19), 1805295.

(2) Kageyama, H.; Hayashi, K.; Maeda, K.; Attfield, J. P.; Hiroi, Z.; Rondinelli, J. M.; Poeppelmeier, K. R. Expanding Frontiers in Materials Chemistry and Physics with Multiple Anions. *Nat. Commun.* **2018**, *9* (1), 02838-4 DOI: 10.1038/s41467-018-02838-4.

(3) Pan, Y.; Guo, S.-P.; Liu, B.-W.; Xue, H.-G.; Guo, G.-C. Second-Order Nonlinear Optical Crystals with Mixed Anions. *Coord. Chem. Rev.* **2018**, *374*, 464−496.

(4) Yang, M.; Oró-Solé, J.; Kusmartseva, A.; Fuertes, A.; Attfield, J. P. Electronic Tuning of Two Metals and Colossal Magnetoresistances in $EuWO_{1+x}N_{2-x}$ Perovskites. *J. Am. Chem. Soc.* **2010**, *132* (13), 4822−4829.

(5) Tran, T. T.; Gooch, M.; Lorenz, B.; Litvinchuk, A. P.; Sorolla, M. G.; Brgoch, J.; Chu, P. C. W.; Guloy, A. M. $Nb_2O_2F_3$: A Reduced Niobium (III/IV) Oxyfluoride with a Complex Structural, Magnetic, and Electronic Phase Transition. *J. Am. Chem. Soc.* **2015**, *137* (2), 636−639.

(6) Khamari, B.; Nanda, B. R. K. Shifting of Fermi Level and Realization of Topological Insulating Phase in the Oxyfluoride $BaBiO_2F$. *Mater. Res. Express* **2019**, *6* (6), No. 066309.

(7) Attfield, J. P. Principles and Applications of Anion Order in Solid Oxynitrides. *Cryst. Growth Des.* **2013**, *13* (10), 4623−4629.

(8) Tsujimoto, Y.; Yamaura, K.; Uchikoshi, T. Extended Ni(III) Oxyhalide Perovskite Derivatives: Sr_2NiO_3X (X = F, Cl). *Inorg. Chem.* **2013**, *52* (17), 10211−10216.

(9) Kubo, A.; Giorgi, G.; Yamashita, K. Anion Ordering in CaTaO2N: Structural Impact on the Photocatalytic Activity. Insights from First-Principles. *Chem. Mater.* **2017**, *29*, 539−545.

(10) Le Berre, F.; Crosnier-Lopez, M.-P.; Galven, C.; Fourquet, J.-L.; Legein, C.; Body, M.; Buzaré, J.-Y. Ca^{2+} /Vacancies and O^{2-}/F^{-} Ordering in New Oxyfluoride Pyrochlores $Li_{2x}Ca_{1.5-x}\square_{0.5-x}M_2O_6F$ (M = Nb,Ta) for $0 \leq x \leq 0.5$. *Dalton Trans.* **2007**, No. 23, 2457−2466.

(11) Sronek, L.; Lhoste, J.; Gaudon, M.; Legein, C.; Buzaré, J.-Y.; Body, M.; Criniere, G.; Tressaud, A.; Pechev, S.; Demoùrgues, A. Probing the Local Environments of Fluorine in Ce-Based Fluorite-Type Oxyfluorides with ^{19}F MAS NMR Spectroscopy. *J. Phys. Chem. C* **2008**, *112* (3), 860−866.

(12) Du, L.-S.; Wang, F.; Grey, C. P. High-Resolution ^{19}F MAS and ^{19}F−^{113}Cd REDOR NMR Study of Oxygen/Fluorine Ordering in Oxyfluorides. *J. Solid State Chem.* **1998**, *140* (2), 285−294.

(13) Du, L.-S.; Samoson, A.; Tuherm, T.; Grey, C. P. ^{19}F/^{23}Na Double Resonance MAS NMR Study of Oxygen/Fluorine Ordering in the Oxyfluoride $Na_5W_3O_9F_5$. *Chem. Mater.* **2000**, *12* (12), 3611−3616.

(14) Choy, J.-H.; Kim, J.-Y.; Kim, S.-J.; Sohn, J.-S.; Han, O. H. New Dion−Jacobson-Type Layered Perovskite Oxyfluorides, $ASrNb_2O_6F$ (A = Li, Na, and Rb). *Chem. Mater.* **2001**, *13* (3), 906−912.

(15) Im, W. B.; George, N.; Kurzman, J.; Brinkley, S.; Mikhailovsky, A.; Hu, J.; Chmelka, B. F.; DenBaars, S. P.; Seshadri, R. Efficient and Color-Tunable Oxyfluoride Solid Solution Phosphors for Solid-State White Lighting. *Adv. Mater.* **2011**, *23* (20), 2300−2305.

(16) Du, L.-S.; Schurko, R. W.; Kim, N.; Grey, C. P. Solid-State ^{93}Nb, ^{19}F, and ^{113}Cd Nuclear Magnetic Resonance Study of Niobium Oxyfluorides: Characterization of Local Distortions and Oxygen/Fluorine Ordering. *J. Phys. Chem. A* **2002**, *106* (34), 7876−7886.

(17) Krylov, A. S.; Sofronova, S. N.; Kolesnikova, E. M.; Ivanov, Yu. N.; Sukhovsky, A. A.; Goryainov, S. V.; Ivanenko, A. A.; Shestakov, N. P.; Kocharova, A. G.; Vtyurin, A. N. Experimental and Theoretical Methods to Study Structural Phase Transition Mechanisms in K3WO3F3 Oxyfluoride. *J. Solid State Chem.* **2014**, *218*, 32−37.

(18) Laptash, N. M.; Udovenko, A. A. On the Identification of Oxygen and Fluorine Atoms in Disordered Inorganic Oxyfluoride Compounds. *J. Struct. Chem.* **2016**, *57* (2), 390−398.

(19) Holland, M.; Charles, N.; Rondinelli, J. M.; Poeppelmeier, K. R. Reconstructive Transitions from Rotations of Rigid Heteroanionic Polyhedra. *J. Am. Chem. Soc.* **2016**, *138* (36), 11882−11889.
(20) Pinlac, R. A. F.; Stern, C. L.; Poeppelmeier, K. R. New Layered Oxide-Fluoride Perovskites: KNaNbOF5 and KNaMO2F4 (M = Mo6+, W6+). *Crystals* **2011**, *1* (1), 3−14.
(21) Kavun, V. Ya.; Kozlova, S. G.; Laptash, N. M.; Tkachenko, I. A.; Gabuda, S. P. Tricritical Point in Ferroelastic Ammonium Titanyl Fluoride: NMR Study. *J. Solid State Chem.* **2010**, *183* (9), 2218−2221.
(22) Marvel, M. R.; Lesage, J.; Baek, J.; Halasyamani, P. S.; Stern, C. L.; Poeppelmeier, K. R. Cation−Anion Interactions and Polar Structures in the Solid State. *J. Am. Chem. Soc.* **2007**, *129* (45), 13963−13969.
(23) Chang, K. B.; Vinokur, A.; Pinlac, R. A. F.; Suchomel, M. R.; Marvel, M. R.; Poeppelmeier, K. R. How Lewis Acidity of the Cationic Framework Affects KNaNbOF $_5$ Polymorphism. *Inorg. Chem.* **2014**, *53* (13), 6979−6984.
(24) Vonrüti, N.; Aschauer, U. Epitaxial strain dependence of band gaps in perovskite oxynitrides compared to perovskite oxides. *Physical Review Materials* **2018**, *2*, 105401.
(25) Bertolini, J. C. Hydrofluoric Acid: A Review of Toxicity. *Journal of Emergency Medicine* **1992**, *10* (2), 163−168.
(26) Peters, D.; Miethchen, R. Symptoms and Treatment of Hydrogen Fluoride Injuries. *J. Fluorine Chem.* **1996**, *79* (2), 161−165.
(27) Segal, E. B. First Aid for a Unique Acid, HF: A Sequel. *Chem. Health Saf.* **2000**, *7* (1), 18−23.
(28) Harrison, W. T. A.; Nenoff, T. M.; Gier, T. E.; Stucky, G. D. Tetrahedral-Atom 3-Ring Groupings in 1-Dimensional Inorganic Chains: Beryllium Arsenate Hydroxide Hydrate (Be2AsO4OH.Cntdot.4H2O) and Sodium Zinc Hydroxide Phosphate Hydrate (Na2ZnPO4OH.Cntdot.7H2O). *Inorg. Chem.* **1993**, *32* (11), 2437−2441.
(29) Ernst, H.; Freude, D.; Mildner, T.; Wolf, I. Laser-Supported High-Temperature MAS NMR for Time-Resolved in Situ Studies of Reaction Steps in Heterogeneous Catalysis. *Solid State Nucl. Magn. Reson.* **1996**, *6* (2), 147−156.
(30) Thurber, K. R.; Tycko, R. Measurement of Sample Temperatures under Magic-Angle Spinning from the Chemical Shift and Spin-Lattice Relaxation Rate of 79Br in KBr Powder. *J. Magn. Reson.* **2009**, *196* (1), 84−87.
(31) Kresse, G.; Furthmüller, J. Efficient Iterative Schemes for *Ab Initio* Total-Energy Calculations Using a Plane-Wave Basis Set. *Phys. Rev. B: Condens. Matter Mater. Phys.* **1996**, *54* (16), 11169−11186.
(32) Vasiliev, A. D.; Laptash, N. M. Polymorphism of KNaNbOF5 Crystals. *J. Struct. Chem.* **2012**, *53* (5), 902−906.
(33) Blöchl, P. E. Projector Augmented-Wave Method. *Phys. Rev. B: Condens. Matter Mater. Phys.* **1994**, *50* (24), 17953−17979.
(34) Perdew, J. P.; Burke, K.; Ernzerhof, M. Generalized Gradient Approximation Made Simple. *Phys. Rev. Lett.* **1996**, *77* (18), 3865−3868.
(35) Pickard, C. J.; Mauri, F. All-Electron Magnetic Response with Pseudopotentials: NMR Chemical Shifts. *Phys. Rev. B: Condens. Matter Mater. Phys.* **2001**, *63* (24), 245101 DOI: 10.1103/PhysRevB.63.245101.
(36) Yates, J. R.; Pickard, C. J.; Mauri, F. Calculation of NMR Chemical Shifts for Extended Systems Using Ultrasoft Pseudopotentials. *Phys. Rev. B: Condens. Matter Mater. Phys.* **2007**, *76* (2), 024401 DOI: 10.1103/PhysRevB.76.024401.

https://dx.doi.org/10.1021/acs.chemmater.0c01439
Chem. Mater. 2020, 32, 5715−5722